Pergamon

Int. J. Heat Mass Transfer. Vol. 37, No. 3, pp. 461–468, 1994

0017–9310/94 $6.00 + 0.00

Transient mass transfer at the surface of an evaporating stationary droplet

S. M. GHIAASIAAN and D. LUO
George W. Woodruff School of Mechanical Engineering, Georgia Institute of Technology, Atlanta, GA 30332, U.S.A.

(*Received* 19 *October* 1992 *and in final form* 19 *July* 1993)

Abstract—The combined transient heat and mass transfer during the evaporation of a superheated stationary droplet, surrounded by its own saturated vapor, is numerically investigated. The droplet and its surrounding vapor are assumed to contain a tracer amount of the transferred species. The effects of important physical parameters, when the partition coefficient of the transferred species is much larger than one, are examined. It is shown that, over a wide range of parameters, mass transfer is gas-side controlled. The mass transfer resistance associated with the vapor layer resulting from the droplet evaporation controls the droplet–vapor mass transfer, and can reduce the rate, or even reverse the direction, of mass transfer in the droplet.

1. INTRODUCTION

DROPLETS are important in many natural and industrial processes, and have been studied by numerous investigators over several decades. Classical monographs discussing the fundamental aspects of hydrodynamics and transfer processes in droplets include refs. [1, 2]. Reviews of more recent advances can be found in refs. [3, 4]. Certain aspects of hydrodynamics and heat/mass transfer in droplets are not well understood, however, and further studies are underway.

In this paper, an analytical study of the combined, transient heat and mass transfer in a non-circulating droplet is performed. The problem represents a droplet suddenly introduced into a gaseous environment, mainly composed of the droplet saturated vapor, where the pressure is lower than the saturation pressure associated with the droplet temperature. The droplet is assumed to be basically a single-component liquid, containing a small dissolved amount of a volatile substance. No chemical interactions are assumed, and the droplet is assumed stationary, without internal circulation. The gas surrounding the droplet is also stationary, except for the motion induced due to the evaporation.

An example for the application of the stated problem is the transport of radionuclides during a U-tube steam generator tube rupture event in a pressurized water reactor [5]. In this event, the primary-side liquid, which is normally under high pressure, flows through the rupture into the secondary-side of the steam generator, where it flashes and partially evaporates. Some of the unevaporated primary-side liquid is atomized, forming a spray of small droplets. These droplets, which are entrained by the vapor generated due to flashing, undergo further evaporation, and exchange volatile radionuclides with the steam environment in the secondary side. Also, during the steam generator tube rupture events the steam leaving the secondary side of the steam generator may carry small droplets contaminated with volatile radionuclides. These droplets which are typically in the 1–10 μm size range [5], may have a small relative velocity with respect to their surrounding gas, mainly due to gravity. The droplet Reynolds number range is ≈ 1–10. Droplet internal circulation is neglected in this paper. The similar problem for larger droplets ($Re \approx 100$), where the droplet internal circulation is considered, will be addressed in a separate paper [6].

Previous studies have mostly dealt with either external, or internal steady-state heat/mass transfer resistances. Steady-state external resistance models for a slow flow past a rigid spherical body with constant diameter include refs. [2, 7], and can be approximately represented by simple empirical correlations of the form [3]

$$Sh_G = f(Pe_m, Re, \kappa). \quad (1)$$

Similar heat transfer correlations can be obtained by replacing Sh_G with Nu, and Pe_m with Pe. In the limit of $Pe_m \to 0$ (stagnant conditions), $Sh_G = 2$. Steady-state internal resistance models, accounting for the droplet internal circulation, include refs. [8–10].

Various transient cases have also been analytically modeled [11, 12]. Empirical correlations, which approximate numerically-obtained results have also been derived in the following generic form [3]

$$Sh_G = f(Pe_m, \kappa, \tau_{m,G}). \quad (2)$$

Heat or mass transfer between a rigid spherical particle with variable diameter and a gaseous environment was investigated in ref. [13].

An extensive numerical investigation, addressing the combined effects of the internal and external resistances in droplets without internal circulation, has

NOMENCLATURE

C_p	specific heat [J kg^{-1} K^{-1}]
$\mathscr{D}$	mass diffusivity of the trace species [m^2 s^{-1}]
E	evaporation coefficient [—]
erf	error function
H^*	partition coefficient, defined in equation (4)
He	Henry number, defined in equation (7)
h	heat transfer coefficient [W m^{-2} K^{-1}]
$\hat{h}_{fg}$	latent heat of vaporization [J kg^{-1}]
Ja'	modified Jakob number, $C_{PL}(T_L^0 - T_G^\infty)/\hat{h}_{fg}$
K	mass transfer coefficient [kg m^{-2} s^{-1}]
k	thermal conductivity [W m^{-1} K^{-1}]
Le	liquid Lewis number, $\alpha_L/\mathscr{D}_L$
M	normalized mass fraction, m/m_L^0
m	mass fraction
$\mathscr{M}$	molecular mass [kg (k mole)$^{-1}$]
n	evaporation mass flux [kg m^{-2} s^{-1}]
Nu	Nusselt number, $2hR/k_G$
Pe	heat transfer Peclet number, $2R^0u^\infty/\alpha_G$
Pe'_G	modified Peclet number, $(nR^0/\rho_G\mathscr{D}_G)(1-(\rho_G/\rho_L))$
Pe'_L	modified Peclet number, $(nR^0/\rho_L\mathscr{D}_L)$
Pe_m	mass transfer Peclet number, $2R^0u^\infty/\mathscr{D}_G$
$\mathscr{R}$	universal gas constant [J (k mole)$^{-1}$ K^{-1}]
R	droplet radius [m]
r	radial coordinate [m]
Re	Reynolds number, $2\rho_G u^\infty R/\mu_G$
Sc_L	liquid-side Schmidt number, $\nu_L/\mathscr{D}_L$
Sh_L	liquid-side Sherwood number, $2K_LR/\rho_L\mathscr{D}_L$
Sh_G	gas-side Sherwood number, $2K_GR/\rho_G\mathscr{D}_G$
T	temperature [K]
t	time [s]
u	velocity [m s^{-1}]
X	mole fraction of transferred species.

Greek symbols

α	thermal diffusivity [m^2 s^{-1}]
β	dimensionless parameter defined as $\rho_G\mathscr{D}_G/\rho_L\mathscr{D}_L$
ζ	transformed radial coordinate, $\ln\eta$
η	dimensionless radial coordinate, r/R
θ	superheat temperature, $T_L - T_{sat}$ [K]
κ	viscosity ratio, μ_L/μ_G
μ	kinematic viscosity [kg m^{-1} s^{-1}]
ρ	density [kg m^{-3}]
ρ^*	partial density of the transferred species [kg m^{-3}]
τ	dimensionless time, $t\alpha_L/(R^0)^2$
$\tau_{m,G}$	dimensionless time, $t\mathscr{D}_G/(R^0)^2$
$\tau_{m,L}$	dimensionless time, $t\mathscr{D}_L/(R^0)^2$
Ω	dimensionless temperature in the droplet, θ/θ^0.

Subscripts

G	gas-side
L	liquid-side
m	mass transfer
s	s-surface (Fig. 1)
sat	saturation
u	u-surface (Fig. 1).

Superscripts

—	average
∞	infinitely far from droplet
0	initial.

been reported by Brauer [14, 15] for spherical particles with constant diameter, and by Schirrmann [16] for spherical particles with variable diameter. Brauer [15] numerically solved two-dimensional (r, θ) species conservation equations, inside and outside spherical droplets, for stagnant and flowing gas conditions. In the latter case, the hydrodynamics were assumed steady-state. The velocity profiles were obtained from the Hadamard–Rybczynski [17] solution for creep flow, and from a numerical solution of the fluid momentum conservation equations for high Reynolds numbers. Based on his numerical results, Brauer derived correlations, separately for internal and external resistances in the form:

$$\frac{\bar{m}_L\rho_L - H^*m_G^\infty\rho_G}{(m_L\rho_L)^0 - H^*m_G^\infty\rho_G} = f(\tau_{m,L}, \tau_{m,G}, H^*) \quad (3)$$

where

$$H^* = \frac{\rho_u^*}{\rho_s^*} \quad (4)$$

$$\rho_u^* = m_u\rho_L \quad (5)$$

$$\rho_s^* = m_s\rho_G. \quad (6)$$

Equation (4) represents equilibrium at the interphase, and H^* is called the partition coefficient or distribution factor by some [3, 18–20] and Henry number by others [14–16]. In this paper, H^* is referred to as the partition coefficient, and [21]

$$He = X_s/X_u. \quad (7)$$

When $m_L \ll 1$ and $m_G \ll 1$, H^* and He are related according to

$$H^* = \rho_L\mathscr{M}_G/(\rho_G\mathscr{M}_L He) \quad (8)$$

where $\mathcal{M}_G$ and $\mathcal{M}_L$ are identical when the liquid is surrounded by its own pure vapor.

Following the approach of Brauer [14, 15], Schirrmann [16] performed numerical calculations representing mass transfer at the interphase of a single-species stationary spherical particle with a variable volume, surrounded by a stagnant gas. The numerical model was one-dimensional (r), and the volume change was only due to the transferred species.

The evaporation of single and multicomponent fossil fuel droplets in combustors has been the subject of intense investigations recently. Droplets which result from shattering of high-velocity fuel jets injected into combustors are typically assumed about 100 μm in diameter with $Re \approx 100$, and evaporate in a very hot gaseous environment, typically several hundred K hotter than the droplet. Sensible heat transfer from the gas provides for droplet evaporation. Existing numerical models mostly assume steady-state hydrodynamics and heat and mass transfer in the gas phase [22–27]. They also either assume a rigid droplet [24, 26] or assume steady-state droplet internal circulation similar to Hill's vortex flow [22, 23, 25, 28, 29]. These assumptions are adequate when the characteristic time periods representing the establishment of quasi-steady state hydrodynamics in the liquid and gas phases are much smaller than the characteristic time period representing droplet cooling. Orders of magnitude of these characteristic time periods depend on droplet Re [22]. When $Re \approx 100$ the quasi-steady state hydrodynamics assumption is adequate [22]. However, for the droplets studied here the characteristic time representing the establishment of quasi-steady hydrodynamics is typically larger than the droplet characteristic cooling time period. More recently a numerical droplet evaporation model using fully-transient one or two dimensional conservation equations inside and outside the droplet has been introduced [30], which assumes a laminar or quiescent gas. In all of the models dealing with the evaporation of fuel droplets, the droplet-gas sensible heat transfer is significant, and property variations with temperature are important during the droplet life time. Neither of these effects is significant in the problem addressed in this paper.

2. MATHEMATICAL MODEL

Figure 1(a) depicts the assumed droplet, and Fig. 1(b) is a schematic of the droplet–vapor interphase. The mass fraction profiles in Fig. 1(b) represent conditions where mass is transferred from the gas into the liquid, with negligible evaporation or condensation. Evaporation, as will be shown in Section 4, significantly modifies these profiles. The droplet is initially at $T_L^0 > T_{sat}$, and contains a dissolved volatile species with initial mass fraction $m_L^0 \ll 1$. At time $t = 0$ the droplet is introduced into the depicted environment containing droplet vapor at $T_G^\infty = T_{sat}(P)$, where P is the ambient pressure. The vapor

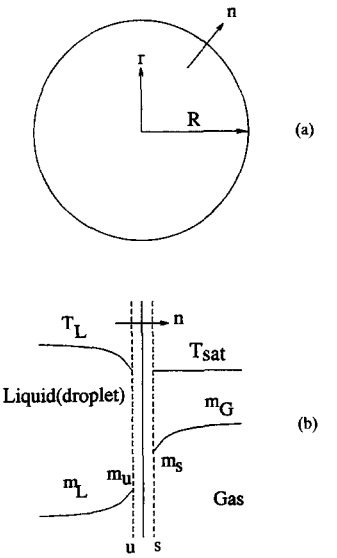

FIG. 1. Schematic of the droplet and the gas–liquid interphase. (a) Droplet. (b) The gas–liquid interphase.

phase contains the volatile species with mass fraction $m_G^\infty \ll 1$. The gas is assumed infinitely large, with no chemical reactions. The effect of interphase curvature on the equilibrium vapor pressure (Kelvin effect) is neglected. Liquid and gas are both assumed incompressible, and their thermophysical properties are assumed independent of temperature. This is a reasonable assumption since the initial droplet superheat is small, typically $\approx$2–10 K. Spherical symmetry is assumed, and no flow, other than that induced by evaporation, is assumed.

2.1. *Heat transfer*

The dimensionless transient heat conduction in the droplet can be represented by

$$\gamma^2 \frac{\partial \Omega}{\partial \tau} - \gamma \left(\frac{d\gamma}{d\tau}\right) \eta \frac{\partial \Omega}{\partial \eta} = \frac{1}{\eta^2} \frac{\partial}{\partial \eta} \left(\eta^2 \frac{\partial \Omega}{\partial \eta}\right). \quad (9)$$

The second term on the left hand side represents the effect of the moving interphase due to evaporation. The initial condition, and symmetry at droplet center, give:

$$\Omega = 1 \quad \text{at } 0 \leqslant \eta \leqslant 1, \tau \leqslant 0 \quad (10)$$

$$\frac{\partial \Omega}{\partial \eta} = 0 \quad \text{at } \eta = 0, \tau > 0. \quad (11)$$

At the surface of the droplet, and for a very short period of time following the initiation of the transient, the interphase resistance to heat transfer is significant. Using the simple kinetic theory of gases for calculating the evaporation mass flux, there results [31, 32]

$$\frac{\partial \Omega}{\partial \eta} = -\frac{R^0 \gamma}{\rho_L \alpha_L Ja'} n \quad \text{at } \eta = 1, \tau > 0 \quad (12)$$

$$n = E\sqrt{\left(\frac{\mathscr{M}}{2\pi\mathscr{R}}\right)}\left[\frac{P_{sat}(T_u)}{\sqrt{T_u}} - \frac{P}{\sqrt{T_s}}\right] \quad (13)$$

where $\mathscr{M}$ is the molecular mass of the liquid, and T_u is related to Ω according to:

$$\Omega = (T_u - T_{sat})/(T_L^0 - T_{sat}) \quad \text{at } \eta = 1. \quad (14)$$

Following Maa [31], $E = 1$ is assumed.

Equation (13) neglects the interphase curvature, since the droplet diameters considered here are at least two orders of magnitude larger than the mean free path of the vapor molecules. The temperature difference between the gas-side surface of the Knudsen layer (the s-surface) and the ambient vapor, $T_s - T_{sat}$, is negligibly small during evaporation from, or condensation on, a liquid droplet surrounded by its own pure saturated vapor [33]. Accordingly, $T_s = T_{sat}$, and sensible heat transfer between the droplet and vapor is negligible.

When the interphase resistance is neglected, equation (12) is replaced with:

$$\Omega = 0 \quad \text{at } \eta = 1, \tau > 0. \quad (15)$$

Energy conservation at the interphase results in

$$\frac{d\gamma}{d\tau} = \frac{Ja'}{\gamma}\left.\frac{\partial\Omega}{\partial\eta}\right|_{\eta=1}. \quad (16)$$

2.2. *Mass transfer*

Mass conservation for the transferred trace species in the liquid phase is governed by

$$\gamma^2\frac{\partial M_L}{\partial\tau_{m,L}} - \gamma\left(\frac{d\gamma}{d\tau_{m,L}}\right)\eta\frac{\partial M_L}{\partial\eta} = \frac{1}{\eta^2}\frac{\partial}{\partial\eta}\left(\eta^2\frac{\partial M_L}{\partial\eta}\right). \quad (17)$$

Mass balance on the interphase, furthermore, gives

$$u_{G|r=R} = \left[1 - \frac{\rho_G}{\rho_L}\right]\frac{n}{\rho_G}. \quad (18)$$

Since the gas is assumed incompressible, the gas velocity varies with η according to

$$u_G(r) = u_{G|r=R}\eta^{-2}. \quad (19)$$

The species mass conservation equation in the gas phase is then

$$\gamma^2\frac{\partial M_G}{\partial\tau_{m,G}} + \left[\frac{1}{\eta^2}Pe'_G\gamma - \gamma\left(\frac{d\gamma}{d\tau_{m,G}}\right)\eta\right]\frac{\partial M_G}{\partial\eta} = \frac{1}{\eta^2}\frac{\partial}{\partial\eta}\left(\eta^2\frac{\partial M_G}{\partial\eta}\right). \quad (20)$$

The first term in the bracket on the left hand side of equation (20) represents convection. Initial and boundary conditions for equations (17) and (20) are as follows:

$$M_L = 1 \quad \text{at } 0 \leqslant \eta \leqslant 1, \tau \leqslant 0 \quad (21)$$

$$\frac{\partial M_L}{\partial\eta} = 0 \quad \text{at } \eta = 0, \tau > 0 \quad (22)$$

$$M_L = M_u \quad \text{at } \eta = 1, \tau > 0 \quad (23)$$

$$M_G = M_G^x = \frac{m_G^\infty}{m_L^0} \quad \text{at } 1 < \eta < \infty, \tau \leqslant 0 \quad (24)$$

$$M_G = M_G^\infty \quad \text{at } \eta \to \infty \quad (25)$$

$$M_G = M_s \quad \text{at } \eta = 1, \tau > 0. \quad (26)$$

The liquid-side and gas-side concentrations of the transferred species at the interphase are related through equilibrium at the interphase according to equation (7). Since $X_s \ll 1$ and $X_u \ll 1$, they can be replaced in equation (7) with m_s and m_u, respectively, giving

$$M_s = He\,M_u. \quad (27)$$

Mass conservation for the transferred species at the interphase gives, at $r = R$:

$$nm_L - \rho_L\mathscr{D}_L\frac{\partial m_L}{\partial r} = nm_G - \rho_G\mathscr{D}_G\frac{\partial m_G}{\partial r}. \quad (28)$$

Equations (27) and (28) are now combined and nondimensionalized to get, at $\eta = 1$,

$$Pe'_L\gamma(1-He)M_L - \frac{\partial M_L}{\partial\eta} + \beta\frac{\partial M_G}{\partial\eta} = 0. \quad (29)$$

3. METHOD OF SOLUTION

3.1. *The limiting case of $Ja' \to 0$ and $\tau \to 0$*

In the limit of $Ja' \to 0$, the droplet radius remains constant, and in the limit of $\tau \to 0$, furthermore, the interphase curvature can be neglected. Mass transfer in each phase is then identical to diffusion from a plane (interphase) into a semi-infinite region. It can then be shown that

$$M_G = \left[1 + He\frac{\rho_G}{\rho_L}\sqrt{\left(\frac{\mathscr{D}_G}{\mathscr{D}_L}\right)}\right]^{-1} \times\left\{He\left(M_G^\infty\frac{\rho_G}{\rho_L}\sqrt{\left(\frac{\mathscr{D}_G}{\mathscr{D}_L}\right)} + 1\right) + (M_G^\infty - He)\,\mathrm{erf}\left(\frac{\eta-1}{2\sqrt{(\tau_{m,G})}}\right)\right\} \quad (30)$$

$$M_L = 1 + \left[1 + He\frac{\rho_G}{\rho_L}\sqrt{\left(\frac{\mathscr{D}_G}{\mathscr{D}_L}\right)}\right]^{-1} \times\left[(M_G^\infty - He)\frac{\rho_G}{\rho_L}\sqrt{\left(\frac{\mathscr{D}_G}{\mathscr{D}_L}\right)}\right] \times\left[1 - \mathrm{erf}\left(\frac{1-\eta}{2\sqrt{(\tau_{m,L})}}\right)\right] \quad (31)$$

$$M_u = \left[1 + He\frac{\rho_G}{\rho_L}\sqrt{\left(\frac{\mathscr{D}_G}{\mathscr{D}_L}\right)}\right]^{-1}\left[1 + M_G^\infty\frac{\rho_G}{\rho_L}\sqrt{\left(\frac{\mathscr{D}_G}{\mathscr{D}_L}\right)}\right] \quad (32)$$

$$Sh_L = -\frac{2}{\bar{M}_L - M_u}\left.\frac{\partial M_L}{\partial \eta}\right|_{\eta=1} = \frac{2}{\sqrt{(\pi\tau_{m,L})}} \quad (33)$$

$$Sh_G = -\frac{2}{M_s - M_G^\infty}\left.\frac{\partial M_G}{\partial \eta}\right|_{\eta=1} = \frac{2}{\sqrt{(\pi\tau_{m,G})}}. \quad (34)$$

3.2. *Numerical solution*

Equations (9), (17) and (20) were numerically solved by the finite-difference method, using the fully-implicit approach. When equation (12) was used as a boundary condition, however, the quantity n on the right hand side of this equation was assigned its explicit value from the previous time step. Euler's method was used in the solution of equation (16). The time step size, Δt, was identical for all four equations. A uniform-sized mesh was used in equations (9) and (17). Equation (9), however, was solved using fewer mesh points.

Equation (20) was recast in the $(\tau_{m,G}, \zeta)$ coordinates, where $\eta = \exp(\zeta)$, in order to use smaller spacing near the surface of the droplet. Equal spacing in ζ was then applied. The boundary condition at $\eta \to \infty$, equation (25), was imposed at $\zeta = 5$. The spatial derivatives were central differenced. The droplet energy equation was solved using 100 mesh points. For mass transfer, 200 mesh points inside, and 200 outside the droplet were used. The effect of further increasing the number of mesh points was found negligibly small.

The time step was varied during each numerical run, from $\Delta t = 2.5 \times 10^{-8}$ s at the beginning of a transient calculation, to 10^{-6} s near the end. These time step sizes, as will be demonstrated later, provided adequately small numerical errors.

All thermophysical properties were assumed independent of temperature.

4. RESULTS AND DISCUSSION

The properties chosen for the results to be presented are for a superheated water droplet, with $R^0 = 25$ μm, undergoing evaporation cooling in an ambient pressure of 70 atm. Therefore $\rho_L = 740$ kg m^{-3}, $\rho_G = 36.5$ kg m^{-3}, $\hat{h}_{fg} = 1.505 \times 10^6$ J kg^{-1}, and $\alpha_L = 1.43 \times 10^{-7}$ m^2 s^{-1}. For this droplet $Re \approx 5$ for the terminal velocity due to gravity. The properties of the transferred species were varied parametrically, representing the estimated transport properties of iodine in water and steam. The release of radioiodine is an important concern in certain nuclear reactor incidents, in particular during a U-tube steam generator tube rupture (SGTR) incident in pressurized water reactors. At 70 atm which represents the typical operating pressure in the secondary side of a steam generator, for iodine, $\mathscr{D}_L \approx 2.4 \times 10^{-8}$ m^2 s^{-1} and $\mathscr{D}_G \approx 5.0 \times 10^{-7}$ m^2 s^{-1} are estimated [5]. The magnitude of the partition coefficient, however, is not accurately known, and may depend on the water pH and iodine concentration [34]. The expected prototypical value has been estimated to be of the order of 10^2 to 10^4 for parametric and sensitivity calculations relevant to SGTR incidents [5]. The assumed properties were thus varied in the range $10^{-9} \leqslant \mathscr{D}_L \leqslant 10^{-4}$ m^2 s^{-1}; $10^{-9} \leqslant \mathscr{D}_G \leqslant 10^{-5}$ m^2 s^{-1}, and $50 \leqslant H^* \leqslant 5 \times 10^3$. The primary coolant in a pressurized water reactor is subcooled water at typically 150 atmosphere pressure. The initial droplet superheat associated with this example is therefore $\approx$10–30 K. Thus, the droplet initial superheat was varied in the range $0.02 \leqslant \theta_0 \leqslant 50$ K in order to examine the trends and limits of the numerical results.

The effect of time step size, Δt, on the calculated results, was tested, and is represented in Table 1 for a typical run. As noted, choosing $\Delta t = 2.5 \times 10^{-8}$ s at the start of the computations provided adequate convergence. Also depicted in this table is the effect of the interfacial thermal resistance. As noted, the interphase thermal resistance has a relatively small effect on the results. All the results, to be presented below, nevertheless, were obtained using equations (12) and (13) for the droplet surface boundary.

Calculations were compared with Brauer's results [15], for $\hat{h}_{fg} \to \infty$ to maintain a constant droplet radius. These included the results for $H^*(\mathscr{D}_L/\mathscr{D}_G)^{1/2} \ll 1$, $H^* < 1$ and $\mathscr{D}_L/\mathscr{D}_G < 1$, and for $H^*(\mathscr{D}_L/\mathscr{D}_G)^{1/2} \gg 1$, $H^* > 1$ and $\mathscr{D}_L/\mathscr{D}_G > 1$. Agreement was observed in all the cases.

The calculations showed that, for the assumed droplet, evaporation vanishes to a negligibly small amount at $\tau \geqslant 0.5$.

Figure 2 depicts the effect of initial droplet superheat on the transient droplet mean mass fraction, where M_G^∞/He and β are constants. The strong effect of Ja', which represents the interphase evaporation mass flux, is evident. The evaporation mass flux leads to the generation of a film of vapor surrounding the droplet. The concentration of the transferred species in the generated film is significantly different from the bulk vapor, and strongly affects mass transfer in the droplet. The corresponding transferred species mass fraction profiles are depicted in Fig. 3. For $Ja' \leqslant 10^{-2}$ the mass transfer process is similar to desorption from a droplet with constant radius. For higher Ja' the vapor film resulting from the droplet evaporation has a transferred species mass fraction considerably higher than the mass fraction in the bulk vapor, leading to the diffusion of the transferred species away from the droplet surface and into the droplet, and resulting in an increase in the mean droplet mass fraction with time. A quasi-steady profile in the droplet is achieved after evaporation vanishes, represented by the relatively flat profiles in the droplet at $\tau = 1.0$, as depicted in Fig. 3(c). The droplet mass fraction decreases with time following the vanishing of evaporation. Mass desorption, however, is relatively slow, and is controlled by the diffusion in the high concentration vapor layer surrounding the droplet. The latter effect vanishes at $\tau = 50$ (Fig. 2), beyond which the droplet mean mass fraction is independent of Ja'.

Table 1. The effect of time step size and interphase thermal resistance on the calculated droplet mean mass fraction, $\bar{M}_L \cdot H^* = 500$, $M_G^\infty/He = 0.1$, $\mathscr{D}_L = 2.4 \times 10^{-8}\ m^2\ s^{-1}$, $\mathscr{D}_G = 5.0 \times 10^{-7}\ m^2\ s^{-1}$

	$\Delta t(s)$† →			
τ	5×10^{-6}	10^{-7}	2.5×10^{-8}	1×10^{-8}
0.01	1.08748‡ (1.08610)§	1.02378 (1.02245)	1.02328 (1.02198)	1.02322 (1.02189)
0.1	1.11996 (1.11888)	1.05444 (1.05332)	1.05394 (1.05288)	1.05383 (1.05272)
1.0	1.10793 (1.10644)	1.04399 (1.04243)	1.04349 (1.04197)	1.04332 (1.04187)
10.0	0.90799 (0.90701)	0.85919 (0.85819)	0.85888 (0.85767)	0.85878 (0.85759)

† Δt is the time step at the beginning of the computations.

‡ The numbers without parentheses were obtained using equation (12), along with equation (13), to represent the droplet surface boundary condition.

§ Numbers in parentheses were obtained using equation (15) as a boundary condition.

The significance of diffusion in the vapor is further demonstrated in Figs. 4 and 5. Figure 4 depicts the effect of mass diffusivity in the vapor on the droplet mean mass fraction. Initially, when the evaporation mass flux is significant, $\bar{M}_L$ is insensitive to $\mathscr{D}_G/\alpha_L$. After evaporation vanishes, however, mass transfer is controlled by mass diffusion in the vapor. When $\mathscr{D}_G/\alpha_L \gg 1$, the rapid diffusion of the transferred species results in fast dispersal of the high concentration vapor layer surrounding the droplet, as noted in Figs. 5(a)–(c). A quasi-steady profile is obtained at $\tau = 10$ for $\mathscr{D}_G/\alpha_L \gg 1$. Mass transfer in the vapor is much slower when $\mathscr{D}_G/\alpha_L < 1$, resulting in a sustained gas-side controlled, transient desorption.

Figure 6 shows the effects of partition coefficient, and the concentration of the transferred species in the vapor bulk, on mass transfer in the droplet and its vicinity. The droplet mean mass fraction and the transient mass fraction profiles are strongly dependent on both H^* and M_G^∞. In the absence of significant evaporation, M_G^∞/He is the independent parameter representing the effect of bulk vapor mass fraction on mass transfer at the droplet surface (e.g. see equation (3)). Due to evaporation, however, asymptotically similar dependence of $\bar{M}_L$ on M_G^∞/He occurs only when the droplet approaches equilibrium with the vapor bulk.

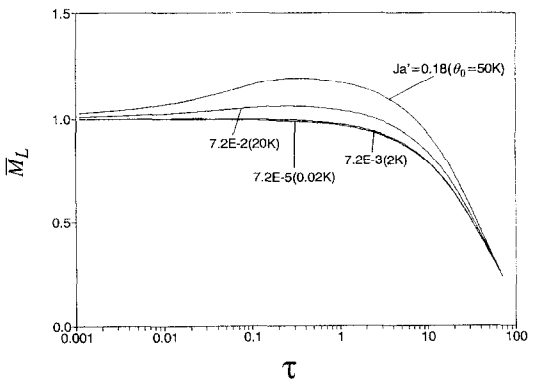

FIG. 2. The effect of droplet initial superheat on the mean droplet mass fraction. $H^* = 5 \times 10^2$, $M_G^\infty/He = 1.0 \times 10^{-2}$ and $\beta = 1.03 \times 10^{-2}$.

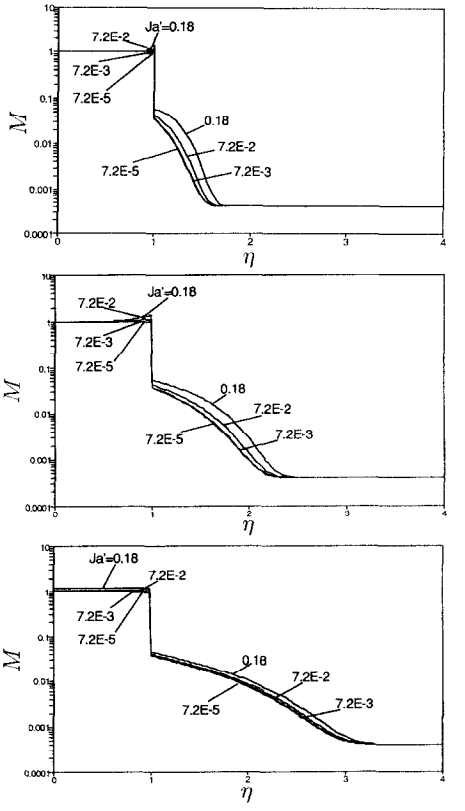

FIG. 3. The effect of droplet initial superheat on mass fraction profiles. (Parameters are similar to Fig. 2.) (a) $\tau = 0.01$; (b) $\tau = 0.1$; (c) $\tau = 1.0$.

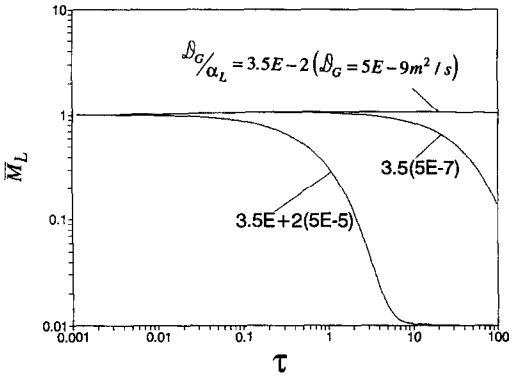

FIG. 4. The effect of the transferred species diffusivity in vapor on the droplet mean mass fraction. $H^* = 5 \times 10^2$, $M_G^\infty/He = 1.0 \times 10^{-2}$, $Le = 5.95$, $Ja' = 7.2 \times 10^{-2}$.

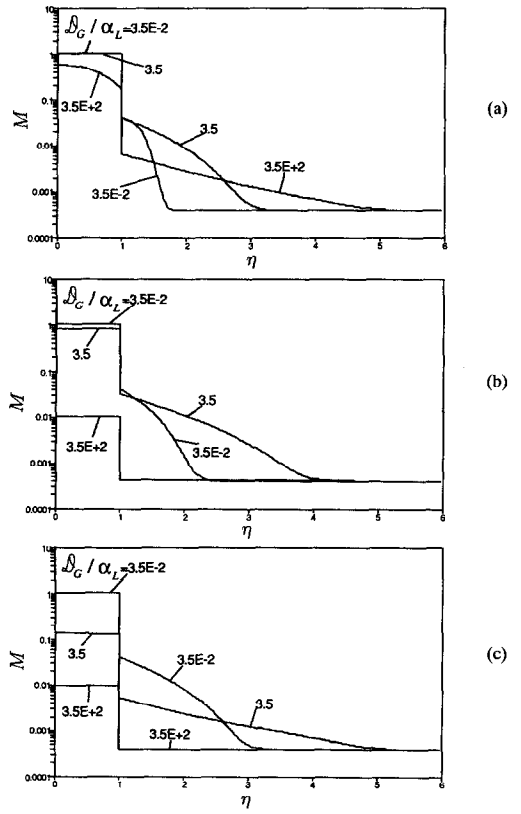

FIG. 5. The effect of the transferred species diffusivity in vapor on the mass fraction profiles. (Parameters are similar to Fig. 4.) (a) $\tau = 1.0$; (b) $\tau = 10$; (c) $\tau = 100$.

The gas-side controlled nature of the process is further demonstrated in Fig. 7, where the sensitivity of the transient droplet mean mass fraction to Le and $\mathscr{D}_G/\alpha_L$ is depicted. These two parameters can alternatively be represented by β. As noted, $\bar{M}_L$ is sensitive to Le only when $\mathscr{D}_G/\alpha_L \gg Le^{-1}$, or, equivalently, when $\beta \gg 1$. For $\beta \leqslant O(1)$, which represents the conditions encountered in most applications, the liquid-side mass diffusivity has a negligible effect for $\tau \leqslant 10^{-2}$, where the mass transfer process is essentially gas-side controlled.

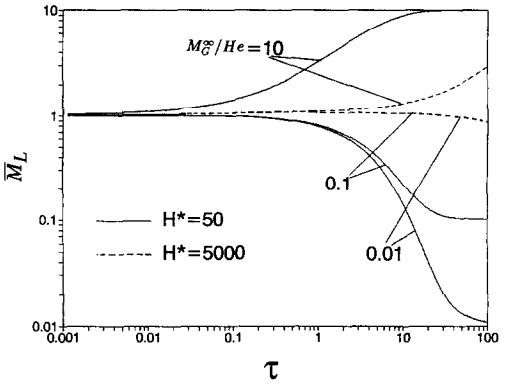

FIG. 6. The effects of the partition coefficient and the transferred species mass fraction in the vapor bulk on the droplet mean mass fraction. $Le = 5.95$, $\mathscr{D}_G/\alpha_L = 3.5$, $Ja' = 7.2 \times 10^{-2}$.

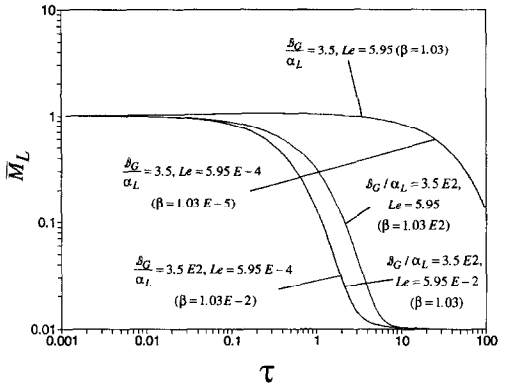

FIG. 7. The effect of the liquid-side mass diffusivity on the droplet mean mass fraction. $H^* = 5 \times 10^2$, $M_G^\infty/He = 1.0 \times 10^{-2}$, $Ja' = 7.2 \times 10^{-2}$.

5. CONCLUSIONS

Mass transfer of a trace, volatile species, associated with an evaporating stagnant droplet, surrounded by the droplet vapor, was numerically modeled. It was shown that the mass transfer process is controlled by the diffusion in the vapor layer generated due to evaporation. The transient mass transfer process is essentially gas-side controlled, except when $\beta \gg 1$.

REFERENCES

1. Sir H. Lamb, *Hydrodynamics*. Cambridge University Press, London (1932).
2. V. E. Levich, *Physico Chemical Hydrodynamics*. Prentice-Hall, Englewood Cliffs, New Jersey (1962).
3. R. Clift, J. R. Grace and M. E. Weber, *Bubbles, Drops, and Particles*. Academic Press, New York (1978).
4. G. Gyarmathy, The spherical droplet in gaseous carrier streams: review and synthesis. In *Multiphase Science and Technology* (Edited by G. F. Hewitt, J. M. Delhaye and N. Zuber), Vol. 1. Hemisphere, Washington, D.C. (1982).
5. S. M. Ghiaasiaan and A. T. Wassel, STARRS-MMS Code: evaluating steam generator tube ruptures, Electric Power Research Institute Report, EPRI NP-6668-CCML, Palo Alto, California (1990).

6. S. M. Ghiaasiaan and D. A. Eghbali, Transient mass transfer of a trace species in an evaporating spherical droplet with internal circulation. To be published.
7. L. Oellrich, H. Schmidt-Traub and H. Brauer, Theoretische berechnung des stofftransports in der umgebung einer eizelblase, *Chem. Engng Sci.* **28,** 711–721 (1973).
8. R. Kronig and J. C. Brink, On the theory of extraction from falling droplets, *Appl. Scient. Res.* **A2,** 142–154 (1951).
9. L. E. Johns and R. E. Beckman, Mechanisms of dispersed-phase mass transfer in viscous, single-drop extraction system, *A.I.Ch.E. Jl* **12,** 10–16 (1966).
10. J. D. Jin and G. L. Borman, A model for multi-component droplet vaporization at high ambient pressures. *Combustion Emission and Analysis*, P-126, 213-223, SAE Inc. (1985).
11. N. Konopliv and E. M. Sparrow, Unsteady heat transfer and temperature for Stokesian flow about a sphere, *J. Heat Transfer* **94C,** 266–272 (1972).
12. B. Abramzon and C. Elata, Unsteady heat transfer from a single sphere in Stokes flow, *Int. J. Heat Mass Transfer* **27,** 687–695 (1984).
13. P. L. T. Brian and H. B. Hales, Effect of transpiration and changing diameter on heat and mass transfer to spheres, *A.I.Ch.E. Jl* **15,** 419–425 (1969).
14. H. Brauer, Unsteady state mass transfer through the interphase of spherical particles—I. Physical and mathematical description of the mass-transfer problem, *Int. J. Heat Mass Transfer* **21,** 445–453 (1978).
15. H. Brauer, Unsteady state mass transfer through the interphase of spherical particles—II. Discussion of results obtained by theoretical models, *Int. J. Heat Mass Transfer* **21,** 455–465 (1978).
16. J. Schirrmann, Unsteady-state mass transfer by fluid particles of changing volume, *Int. J. Heat Mass Transfer* **33,** 253–266 (1990).
17. J. Hadamard, Mouvement permanente lent d'une sphère liquide et visqueuse dans un liquid visqueux, *C.R. Hebd. Séanc. Acad. Sci. Paris* **152,** 1735–1817 (1911).
18. C. C. Lin, Volatility of dilute aqueous solutions, *J. Inorg. Nucl. Chem.* **131,** 1–10 (1981).
19. M. Furrer and R. C. Cripps, Measurement of the iodine partition coefficient, *Nucl. Technol.* **70,** 290–293 (1985).
20. P. W. Marshall, J. B. Lutz and J. L. Kelly, Gamma radiation effects on time-dependent iodine partitioning, *Nucl. Technol.* **76,** 400–407 (1987).
21. D. K. Edwards, V. E. Denny and A. F. Mills, *Transfer Processes* (2nd Edn). Hemisphere, Washington, D.C. (1979).
22. S. Prakash and W. A. Sirignano, Theory of convective droplet vaporization with unsteady heat transfer in circulating liquid phase, *Int. J. Heat Mass Transfer* **23,** 253–268 (1980).
23. B. Abramzon and W. A. Sirignano, Droplet vaporization model for spray combustion calculations, *Int. J. Heat Mass Transfer* **32,** 1605–1618 (1989).
24. C. K. Law, Internal boiling and superheating in vaporizing multicomponent droplets, *A.I.Ch.E. Jl* **24,** 626–632 (1978).
25. A. Y. Tong and W. A. Sirignano, Multicomponent droplet vaporization in a high temperature gas, *Combust. Flame* **66,** 221–235 (1986).
26. A. Makino and C. K. Law, On the controlling parameter in the gasification behavior of multicomponent droplets, *Combust. Flame* **73,** 331–336 (1988).
27. M. Renksizbulut and R. J. Haywood, Transient droplet evaporation with variable properties and internal circulation at intermediate Reynolds numbers, *Int. J. Multiphase Flow* **14,** 189–202 (1988).
28. S. Prakash and W. A. Sirignano, Liquid fuel droplet heating with internal circulation, *Int. J. Heat Mass Transfer* **21,** 885–895 (1978).
29. S. K. Aggarwal, Modeling of a dilute vaporizing multicomponent fuel spray, *Int. J. Heat Mass Transfer* **30,** 1949–1961 (1987).
30. R. J. Haywood, R. Nafziger and M. Renksizbulut, A detailed examination of gas and liquid phase transient processes in convective droplet evaporation, *J. Heat Transfer* **111,** 495–502 (1989).
31. J. R. Maa, Evaporation coefficient of liquids, *Ind. Engng Chem. Fund.* **6,** 504–518 (1967).
32. A. F. Mills and R. A. Seban, The condensation coefficient of water, *Int. J. Heat Mass Transfer* **10,** 1815–1827 (1967).
33. A. F. Mills, Condensation heat transfer: comments on non-equilibrium temperature profiles and the engineering calculation of mass transfer, *Int. J. Multiphase Flow* **6,** 41–50 (1980).
34. E. C. Beahm, S. R. Daish, J. Hopenfeld, W. E. Shockley and P. Voillequé, Iodine speciation and partitioning in PWR steam generator tube rupture, U.S. Nuclear Regulatory Commission Report NUREG-1108 (1985).